Acta Crystallographica Section D
Biological Crystallography
ISSN 0907-4449

Structure of aluminium-bound ovotransferrin at 2.15 Å resolution

Kimihiko Mizutani,[a]* Bunzo Mikami,[b] Shigeo Aibara[a] and Masaaki Hirose[a]

[a]Laboratory of Applied Structural Biology, Division of Applied Life Sciences, The Graduate School of Agriculture, Kyoto University, Uji, Kyoto 611-0011, Japan, and [b]Laboratory of Food Quality Design and Development, Division of Agronomy and Horticultural Science, The Graduate School of Agriculture, Kyoto University, Uji, Kyoto 611-0011, Japan

Correspondence e-mail: kmizutani@kais.kyoto-u.ac.jp

Received 5 August 2005
Accepted 12 October 2005

PDB Reference: aluminium-bound ovotransferrin, 2d3i, r2d3isf.

Transferrin, well known as an iron-transport protein, can bind other metal ions, including toxic ones, and is considered to play an important role in the transportation of such metal ions. Here, a crystal structure of aluminium-bound transferrin is described for the first time. Colourless needle-shaped crystals of aluminium-bound ovotransferrin were obtained in PEG 400 solution. Structural determination was performed by molecular replacement using diferric (iron-bound) ovotransferrin as a model and the structural refinement was performed in the 50–2.15 Å resolution range. The overall organization of the aluminium-bound form is almost the same as the iron-bound form: the protein is folded into two homologous lobes (N- and C-lobes) with two domains; two metal-binding sites are located within the inter-domain clefts of each lobe. Four residues (one Asp, two Tyr and one His) and one bicarbonate anion were found to bind an aluminium ion in either lobe, as in the iron-bound form. The highly similar domain-closed structure of the Al^{3+}-bound form may permit the binding of Al^{3+}-bound transferrin to the transferrin receptor. An unusual interaction, the dilysine trigger, which facilitates iron release at low pH in the endosome, was also found in the Al^{3+}-bound form. These findings support the participation of transferrin in the transport of Al^{3+} ions *in vivo*.

1. Introduction

The major egg-white protein ovotransferrin (oTf) is a member of the transferrin family of iron-binding proteins that includes serum transferrin, lactoferrin and melanotransferrin (Aisen & Listowsky, 1980; Baker *et al.*, 2003). Transferrins serve to control the levels of iron in the body fluids of vertebrates by their ability to bind very tightly two Fe^{3+} ions together with two HCO_3^- ions; serum transferrin can act as the iron transporter to target cells. Ovotransferrin should share the same structural characteristics as hen serum transferrin, since these proteins are derived from the same gene and differ only in their attached carbohydrate (Thibodeau *et al.*, 1978). Although an iron-transport function for oTf in the developing chick embryo has not been proved, specific transferrin–receptor interactions have been demonstrated for egg-white oTf (Brown-Mason & Woodworth, 1984; Mason *et al.*, 1987, 1996). The recent crystal structure of hen serum transferrin (Guha Thakurta *et al.*, 2003; Thakurta *et al.*, 2004) shows an almost indistinguishable main-chain conformation from that of hen oTf (Kurokawa *et al.*, 1995, 1999).

The transferrin molecules are ∼80 kDa single-chain proteins consisting of two homologous N- and C-lobes. Both lobes are further divided into two similarly sized domains (N1 and N2 in the N-lobe; C1 and C2 in the C-lobe; Baker *et al.*, 2003). The two iron-binding sites are located within the inter-

Table 1
Summary of data collection and refinement.

Values in parentheses are for the highest resolution bin.

Crystal data	
Space group	$P2_1$
Unit-cell parameters	
a (Å)	72.35
b (Å)	59.18
c (Å)	87.97
β (°)	95.72
V_M (Å^3 Da^{-1})	2.4
Molecules per ASU	1
Observed reflections	222381
Resolution (Å)	50.0–2.15 (2.23–2.15)
Independent reflections	40021
Completeness (%)	98.4 (94.0)
R_{sym} (%)	8.1 (30.8)
Redundancy	5.6 (5.5)
Mean $I/\sigma(I)$	16.5 (4.2)
Wavelength (Å)	0.8
Refinement statistics	
Resolution limits (Å)	50.0–2.15
No. of reflections used	39956
Completeness (%)	98.4
No. of protein atoms	5189
No. of solvent molecules	270
Ions	2 Al^{3+}, 2 HCO_3^-
Final R factor	0.206
Free R value	0.243
Average B factor (Å^2)	28.9
R.m.s. deviation from ideal geometry	
Bond distances (Å)	0.005
Bond angles (°)	1.2
Dihedrals (°)	22.6
Improper dihedrals (°)	0.73

domain clefts of each lobe. Four of the six Fe^{3+}-coordination sites are occupied by protein ligands (two Tyr residues, one Asp and one His) and the other two by a bidentate bicarbonate anion (Baker *et al.*, 2003). Both lobes of iron-free transferrin have a domain-opened structure and the coordination of the Fe^{3+} ions to two Tyr ligands followed by coordination to the His and Asp ligands converts the open structure into the domain-closed structure of iron-bound transferrin (Guha Thakurta *et al.*, 2003; Thakurta *et al.*, 2004; Kurokawa *et al.*, 1995, 1999; Anderson *et al.*, 1990; Gerstein *et al.*, 1993; Mizutani *et al.*, 1999, 2000, 2001). The movement of the domains can be categorized as a hinge-like motion in which the hinge of each lobe consists primarily of two polypeptide chains (β-strands) linking the domains (Anderson *et al.*, 1990; Gerstein *et al.*, 1993; Mizutani *et al.*, 2001).

Transferrin-dependent Fe^{3+} delivery to the target cells occurs in such a way that the diferric transferrin first binds to the specific receptor that resides on the plasma membrane (Dautry-Varsat *et al.*, 1983). The transferrin–receptor complex is then internalized into the cell and releases Fe^{3+} at acidic pH in the endosome (Dautry-Varsat *et al.*, 1983; Klausner *et al.*, 1983). The iron-dependent conformational change may be closely related to the cellular uptake mechanism of iron; the iron-loaded diferric form shows a higher affinity for the transferrin receptor than does the apo form (Brown-Mason & Woodworth, 1984; Young *et al.*, 1984). The structure of the transferrin receptor–transferrin complex, recently solved by cryo-electron microscopy (Cheng *et al.*, 2004), shows that transferrin interacts with the transferrin receptor through its N1, N2 and C1 domains (Cheng *et al.*, 2004). Since no interaction was found for domain C2, binding to the transferrin receptor does not prevent the opening of the C-lobe and iron release (Cheng *et al.*, 2004).

Since only 20–50% of transferrin is saturated with Fe^{3+} in serum and transferrin can bind other divalent and trivalent metal ions (Cu^{2+}, Al^{3+} *etc.*; Yamamura *et al.*, 1985; Ichimura *et al.*, 1989; Harris & Sheldon, 1990; Li *et al.*, 1996), transferrin may also participate in the transport of other metal ions. Aluminium is unnecessary to cellular activities and is sometimes toxic: high aluminium levels are linked to diseases such as dementia dialitica, iron-adequate microcytic anaemia and osteomalacia (Corain *et al.*, 1996). The accumulation of aluminium was found in the senile plaques of Alzheimer's disease (Roskams & Connor, 1990); however, the participation of transferrin is not clear. Although crystal structures of metal-substituted transferrins are crucial for further understanding, only the crystal structures of Cu^{2+}-, Sm^{3+}- and Ce^{3+}-substituted lactoferrin are known (Smith *et al.*, 1992; Sharma & Singh, 1999; Baker *et al.*, 2000) and no structures of metal-substituted serum transferrin have been reported.

In the present paper, we demonstrate for the first time the crystal structure of Al^{3+}-bound transferrin. The colourless crystals of aluminium-bound ovotransferrin, shown to bind two aluminium ions by inductively coupled plasma-atomic emission spectrometry (ICP-AES), were grown in PEG 400 solution. The crystal structure of Al^{3+}-bound oTf at 2.15 Å resolution was solved by molecular replacement using the structure of diferric (iron-bound) ovotransferrin as a model. The structure of the Al^{3+}-bound form is highly similar to that of the Fe^{3+}-bound form, which may permit the binding of Al^{3+}-bound transferrin to the transferrin receptor and the transport of Al^{3+} ions *in vivo*.

2. Materials and methods

2.1. Materials

Egg-white oTf was purified from fresh hen egg white as described previously (Oe *et al.*, 1988). Other chemicals were guaranteed grade from Wako Pure Chemical Industries (Osaka, Japan), Nacalai Tesque (Kyoto, Japan) and Sigma–Aldrich Chemicals (St Louis, MO, USA).

2.2. Crystallization

Purified oTf (63.2 mg ml^{-1}; 0.8 m*M*) was incubated with 4 m*M* $Al(NO_3)_3$, 8 m*M* nitrilotriacetate and 20 m*M* $NaHCO_3$ in 5 m*M* Tris–HCl pH 8.0; no precipitation was seen in the sample. The sample was diluted to 10 mg ml^{-1} with 5 m*M* Tris–HCl pH 8.0 and crystallized using the sitting-drop vapour-diffusion method. The solution in the crystallization drop was prepared on a polystyrene Micro-Bridge (Hampton Research, Laguna Niguel, CA, USA) by mixing 2 µl protein solution with precipitant solution (15% PEG 400 and 100 m*M* Tris–HCl pH 8.0). The droplets were equilibrated against 1 ml precipitant solution at 277 K. Colourless needle-shaped crys-

tals were obtained within one month, in contrast to crystals of the Fe^{3+}-binding form, which have a deep red colour (Kurokawa *et al.*, 1995).

2.3. Data collection and processing

The crystal was mounted in a nylon cryoloop (Hampton Research) and placed in liquid nitrogen. Diffraction data were collected in a cold nitrogen-gas stream (100 K) using a Jupiter 210 CCD area detector (Rigaku/MSC, TX, USA) with synchrotron radiation at a wavelength of 0.8 Å at the BL38B1 station of SPring-8 (Hyogo, Japan). The resulting data set was processed, merged and scaled using the program package *HKL*2000 to a resolution of 2.15 Å (Table 1).

2.4. Structure refinement

The initial model was obtained by molecular replacement using *AMoRe* from the *CCP*4 program package (Collaborative Computational Project, Number 4, 1994). The protein portion of the structure of diferric (Fe^{3+}-bound) oTf (PDB code 1ovt; Kurokawa *et al.*, 1995) was used as a model. Rigid-body refinement of the four domains (N1, N2, C1 and C2) was carried out using the *CNS* program package (Brünger *et al.*, 1998). Several rounds of restrained least-squares refinement at 2.15 Å resolution followed by manual model building using *TURBO-FRODO* or *Coot* (*WinCoot*; Emsley & Cowtan, 2004) were carried out using *CNS*. Two Al^{3+} ions and two HCO_3^- ions, which were identified from a clear difference density ($F_o - F_c$) map, were included in the model in an early round of refinement (Table 1). The atomic coordinates of the aluminium-bound structure have been deposited with the Protein Data Bank (PDB code 2d3i).

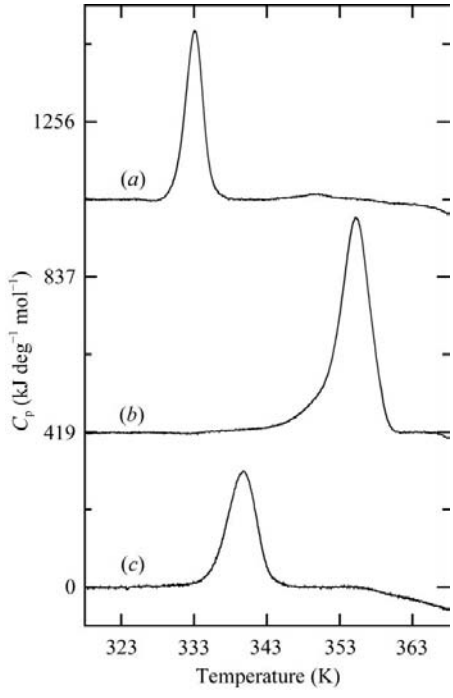

Figure 1
Thermal transition profiles of Al^{3+}-bound oTf. Al^{3+}-bound oTf (oTf incubated with Al^{3+} and $NaHCO_3$) was analyzed using a differential scanning calorimeter as described in the text (*c*). Thermal transition profiles of apo (*a*) and diferric (Fe^{3+}-bound) (*b*) forms of oTf are also shown.

2.5. Differential scanning calorimetry (DSC)

The thermal stabilities of the different forms of oTf (apo, Fe^{3+}-bound and Al^{3+}-bound forms) were analyzed in 0.5 *M* HEPES pH 7.5 using a differential scanning calorimeter (Micro Cal, MCS-DSC, Northampton, MA, USA). The protein concentration was 0.4 mg ml^{-1} and the rate of temperature change was 1 K min^{-1} in the analyses. The data were processed using *Origin* software (Micro Cal).

2.6. Quantitative analyses of bound aluminium and iron

Ovotransferrin (20 mg ml^{-1}; 0.256 m*M*) was incubated with $Al(NO_3)_3$ (4 m*M*), nitrilotriacetate (8 m*M*) and bicarbonate (20 m*M*) in 50 m*M* Tris–HCl pH 8.0 overnight at 277 K. The sample was passed through a Sephadex G-25 column (NAP-10 column, Amersham Biosciences, Piscataway, NJ, USA) twice to remove free metal ions; samples containing 7.77 mg ml^{-1} ovotransferrin were obtained. The same treatment was performed using $FeCl_3$. The samples were diluted tenfold with ultrapure water and quantitative analyses of Al and Fe were performed by ICP-AES at Shimadzu Analytical and Measuring Center, Kyoto, Japan. The wavelengths used were 167.079 and 259.940 nm for aluminium and iron, respectively.

2.7. Evaluation of the extent of domain opening

The width of the metal-binding clefts of the two lobes were quantitatively evaluated by measuring the distances between the centres of gravity of the two domains that form the clefts. Since only the C^α atoms in the respective domains were considered, the centres of gravity correspond to averages of the coordinates (x, y, z). The rotation angles of the domains were calculated by first superposing domain 2 and then finding the additional rotation required to superpose domain 1 (Mizutani *et al.*, 2001). Superposition of structures was carried out using the program *FIT* (Guoguang Lu, Lund University), with only C^α atoms used for the calculations.

3. Results and discussion

3.1. Aluminium-binding capacity

The sample incubated with Al^{3+} and bicarbonate was analyzed by ICP-AES to quantitatively determine the number of bound Al^{3+} ions. The concentration of aluminium in the sample containing 0.77 mg ml^{-1} (0.010 m*M*) ovotransferrin was determined to be 5.51 mg l^{-1}, which corresponds to 1.99 aluminium ions per ovotransferrin molecule. The same analysis was performed for Fe^{3+}: ovotransferrin incubated with Fe^{3+} contained 2.20 molar ratios of iron (1.26 mg l^{-1} iron in 0.77 mg ml^{-1} protein). These values agree well with the expected two metal-binding sites of transferrins.

The thermal stability of oTf incubated with Al^{3+} was analyzed using a differential scanning calorimeter. A single

peak at 340.0 K was found in the thermal transition profile (Fig. 1). Since apo oTf has a single peak at 333.4 K, the peak at 340.0 K should come from Al^{3+}-bound oTf; the increased thermostability also demonstrated the Al^{3+}-binding ability of transferrin. The thermal transition temperature (340.0 K) of the Al^{3+}-bound form is much lower than that of diferric (Fe^{3+}-bound) oTf (355.4 K). The value ΔT_m (difference of the thermal transition temperature between the metal-binding form and the apo form) of the Al^{3+}-bound form and the Fe^{3+}-bound form are 6.6 and 22.0 K, respectively. These ΔT_m values reflect weaker binding of Al^{3+} (Brandts & Lin, 1990; Harris & Sheldon, 1990).

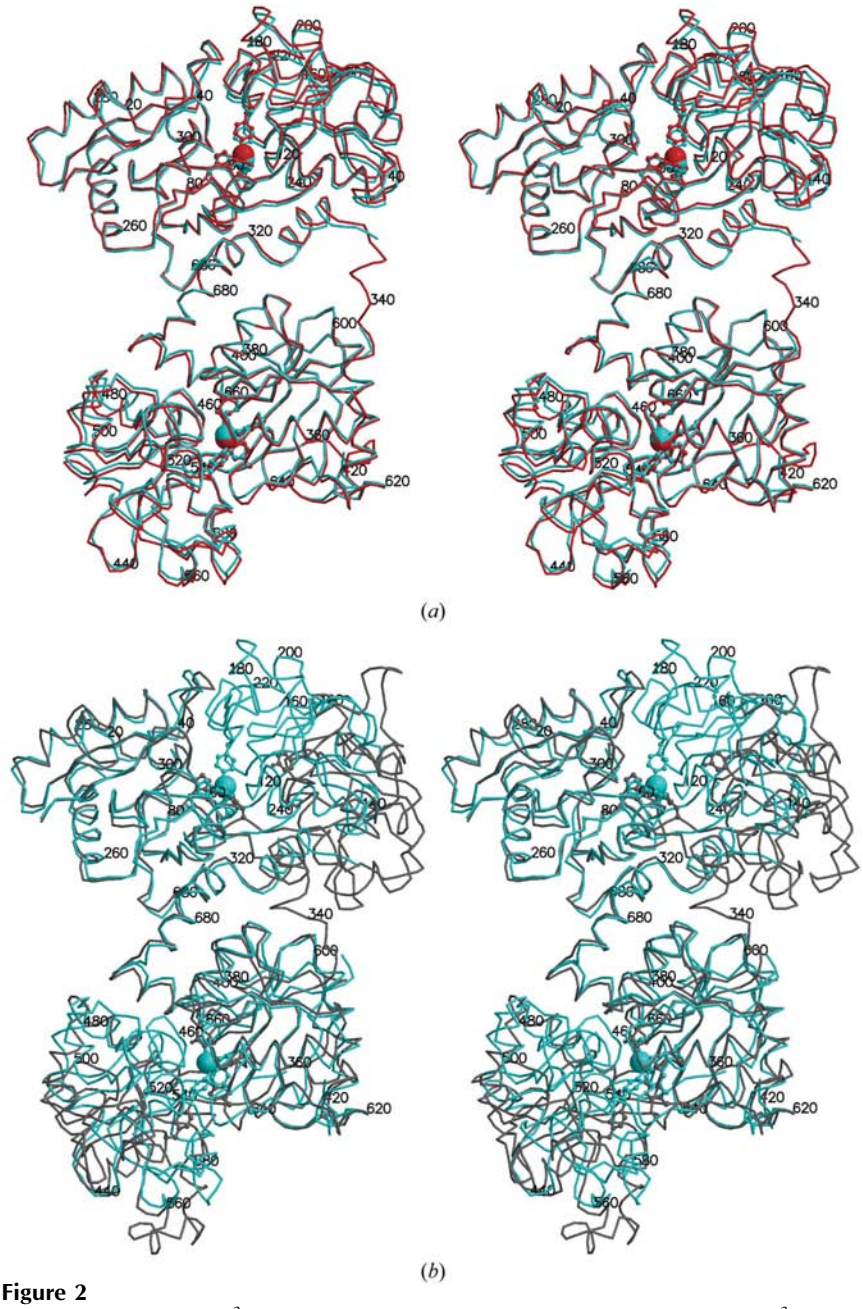

Figure 2
Stereo C^{α} plots of (*a*) Al^{3+}-bound (cyan) and diferric (red) forms of oTf and (*b*) Al^{3+}-bound (cyan) and apo forms (grey). The figures were produced with *MolScript* (Kraulis, 1991) and *Raster3D* (Merritt & Bacon, 1997). The structures were superimposed using the C^{α} atoms of domains N1 and C1. The Al^{3+}-bound, diferric and apo structures were drawn using the present and previous data (Kurokawa *et al.*, 1995, 1999). The residue labels correspond to the Al^{3+}-bound form (except for 340, labelled as in the diferric form or apo form). The Al^{3+} and Fe^{3+} atoms and the side chains of the metal-binding residues are also displayed.

3.2. Quality of the final model

The whole molecule of oTf comprises 686 amino-acid residues. However, residues 1–4, 336–341 and 422–427 are not included in the final model because no clearly interpretable electron density could be seen for these residues. Relevant refinement statistics are given in Table 1. The overall completeness, *R* factor and free *R* values were 98.4%, 0.206 and 0.243, respectively, for data with $F > 0\sigma(F)$. For the highest resolution bin (2.28–2.15 Å), the completeness was 94.4% and the *R* factor and free *R* value were 0.213 and 0.256, respectively. The mean absolute error in atomic position is estimated to be 0.24 and 0.13 Å from Luzzati and σ_A plots, respectively. In a Ramachandran plot of the main-chain torsion angles, 88.5% of the residues are in the core regions, with 99.5% of the residues lying within the allowed regions as defined in the program *PROCHECK*. Of the non-glycine residues, Glu103, Leu299 and Leu636 lie outside the allowed regions. The leucine residues are the central residues in a γ-turn which is conserved in all N- and C-lobes of serum transferrin, oTf and lactoferrin. The glutamic acid residue is also the central residue in a γ-turn.

3.3. Overall organization of the structure

Fig. 2 displays the overall structure of Al^{3+}-bound oTf as a C^{α} trace. The overall structure of the Al^{3+}-bound form was almost the same as that of the diferric (Fe^{3+}-bound) form: as in the diferric oTf structure, the Al^{3+}-bound form is folded into two homologous N- and C-lobes, with each of the lobes divided into two distinct and similarly sized α/β-domains (N1 and N2 in the N-lobe and C1 and C2 in the C-lobe). The two metal-binding sites are located in the clefts formed by the two domains in each lobe and the two domains are linked by two antiparallel β-strands (and a disulfide bond in the C-lobe) that run behind each metal-binding site. The root-mean-square deviations between the Al^{3+}-bound and diferric forms for domains N1 (residues 1–91 and 247–332), N2 (92–246), C1 (343–429 and 589–672) and C2 (430–588) were 0.40, 0.34, 0.45 and 0.71 Å, respectively.

Table 2
Geometry of aluminium-binding sites.

Corresponding values for the Fe^{3+}-bound form (PDB code 1ovt) are shown in parentheses.

	N-lobe	C-lobe
Bond lengths (Å)		
Al—OD1 (Asp60 or 395)	1.94 (2.18)	1.95 (2.34)
Al—OH (Tyr92 or 431)	1.83 (1.84)	2.00 (1.83)
Al—OH (Tyr191 or 524)	1.82 (2.04)	1.71 (1.90)
Al—NE2 (His250 or 592)	2.14 (2.08)	2.05 (2.16)
Al—O1 (bicarbonate)	1.97 (1.85)	2.03 (1.90)
Al—O3 (bicarbonate)	1.93 (2.09)	1.99 (2.14)
Bond angles (°)		
OD1 (Asp60 or 395)—Al—OH (Tyr92 or 431)	87.6 (93.9)	85.2 (88.5)
OD1 (Asp60 or 395)—Al—OH (Tyr191 or 524)	169.2 (173.6)	173.3 (159.4)
OD1 (Asp60 or 395)—Al—NE2 (His250 or 592)	81.6 (88.1)	86.2 (76.7)
OD1 (Asp60 or 395)—Al—O1 (bicarbonate)	94.4 (90.6)	84.8 (90.8)
OD1 (Asp60 or 395)—Al—O3 (bicarbonate)	87.4 (86.2)	85.3 (78.6)
OH (Tyr92 or 431)—Al—OH (Tyr191 or 524)	96.1 (91.0)	100.3 (110.0)
OH (Tyr92 or 431)—Al—NE2 (His250 or 592)	93.9 (89.0)	95.1 (83.0)
OH (Tyr92 or 431)—Al—O1 (bicarbonate)	99.1 (94.6)	90.0 (91.5)
OH (Tyr92 or 431)—Al—O3 (bicarbonate)	164.0 (157.9)	152.9 (149.0)
OH (Tyr191 or 524)—Al—NE2 (His250 or 592)	88.0 (87.9)	89.4 (95.9)
OH (Tyr191 or 524)—Al—O1 (bicarbonate)	95.1 (93.2)	99.0 (97.7)
OH (Tyr191 or 524)—Al—O3 (bicarbonate)	91.6 (90.8)	91.4 (89.1)
NE2 (His250 or 592)—Al—O1 (bicarbonate)	166.3 (176.2)	169.2 (166.4)
NE2 (His250 or 592)—Al—O3 (bicarbonate)	100.5 (113.0)	109.5 (120.3)
O1 (bicarbonate)—Al—O3 (bicarbonate)	66.2 (63.4)	63.9 (61.1)

3.4. Structure of the Al^{3+}-binding sites

The Al^{3+} coordination by four amino-acid residues (Asp60, Tyr92, Tyr191 and His250 in the N-lobe and Asp395, Tyr431, Tyr524 and His592 in the C-lobe) is almost the same as in the diferric form. The distances from Al^{3+} to the four amino-acid residues in each lobe are shown in Table 2. A specific feature of the Al^{3+}-binding sites is that the bond lengths between Al^{3+} and the Asp ligands in each lobe (1.94 and 1.95 Å) are smaller than the bond lengths between Fe^{3+} and those ligands in the diferric form (2.18 and 2.34 Å). As shown in Fig. 3, the electron density shows that bicarbonate is bound as a synergistic anion in both lobes; the bond lengths between Al^{3+} and liganded O atoms (O1 and O3) of the bicarbonate anions are also shown in Table 2. Bicarbonate binding is stabilized through interactions with the protein in the same way as for the diferric form: bicarbonate O1 is hydrogen bonded to Ala123(462) N, bicarbonate O2 to Thr117(456) OG1 and Gly124(463) N and bicarbonate O3 to Arg121(462) NE and NH2 (C-lobe residues in parentheses). The bond angles formed by Al^{3+} and the six ligands of each lobe (Table 2) depart slightly from the ideal 90 or 180° compared with the diferric form.

3.5. Comparison between the Al^{3+}-bound and apo forms

The Al^{3+}-bound structure was compared with the previous apo structure determined at 2.8 Å resolution (Kurokawa *et al.*, 1999). Each of the four domains N1, N2, C1 and C2 has a similar structure in the Al^{3+}-bound and apo forms, although the cleft formed by the two domains is closed in the Al^{3+}-bound form but wide open in the apo form. The extent and mode of the closure are almost the same as in the diferric form: the domains in each lobe rotate around a screw axis passing through the two β-strands linking the domains (Kurokawa *et al.*, 1999; Mizutani *et al.*, 2001). The domains rotate 52.8° (52.4°) around almost the same screw axis and move 2.09 Å (1.85 Å) along the axis for the N-lobe of the Al^{3+}-bound form (and the diferric form). For the C-lobe of the Al^{3+}-bound form (and the diferric form), the rotation angle and translation are 34.6° (34.7°) and 0.36 Å (0.08 Å), respectively.

3.6. Interdomain hydrogen bonds

Interdomain hydrogen bonds (between domains N1 and N2 or between domains C1 and C2) found in the Al^{3+}- and Fe^{3+}-bound forms were calculated from the present coordinates (PDB code 2d3i) and PDB code 1ovt, respectively. Eight hydrogen bonds were found in the N-lobes of the Al^{3+}-bound and Fe^{3+}-bound forms. Two of these are changed between the two forms: Lys296 NZ···Glu215 OE1 and Lys240 NZ···Thr85 OG1 in the Fe^{3+}-bound form change to Lys296 NZ···Asn216 OD1 and Lys296 NZ···Glu215 O in the Al^{3+}-bound form owing to different directions of the two lysine side chains. In the C-lobe, eight and seven hydrogen bonds were found in the Fe^{3+}- and Al^{3+}-bound forms, respectively, and one direct hydrogen bond (Asn632 ND2···Asn548 OD1) in the Fe^{3+}-bound form is changed into an indirect hydrogen bond (through a water molecule) in the Al^{3+}-bound form. An unusual interaction between Lys209 NZ and Lys301 NZ, called the 'dilysine trigger', facilitates iron release at low pH in the endosome (Dewan *et al.*, 1993). This interaction is conserved in the Al^{3+}-bound form (the bond distance is 2.86 Å) and may facilitate release of Al^{3+} at low pH.

4. Discussion

In the study described here, the aluminium-bound structure of oTf has been determined at 2.15 Å resolution as the first demonstration of an Al^{3+}-bound structure of a transferrin. Structures of Cu^{2+}-, Sm^{3+}- and Ce^{4+}-substituted lactoferrins have been reported (Smith *et al.*, 1992; Sharma & Singh, 1999; Baker *et al.*, 2000), but these metal ions have larger ionic radii (Cu^{2+}, 0.73 Å; Sm^{3+}, 0.96 Å; Ce^{4+}, 0.87 Å) than Fe^{3+} (0.65 Å) for six-coordination (Dean, 1999). Since Al^{3+} has an ionic radius of 0.54 Å, our crystal structure is the first demonstration of a smaller metal ion substituted for Fe^{3+} in a transferrin. This study provides important insight into the Al^{3+}-binding mechanism of transferrin and also into the mechanism by which smaller metal ions are bound.

A previous study using X-ray absorption near-edge structure (XANES) spectroscopy reported that aluminium is hexacoordinated in an octahedral-like symmetry in either lobe

of transferrin (Congiu-Castellano *et al.*, 1997). The current crystal structure reveals details of the mode of Al^{3+} binding by transferrin; three O atoms and one N atom of the amino-acid residues (Asp60, Tyr92, Tyr191 and His250 in the N-lobe and Asp395, Tyr431, Tyr524 and His592 in the C-lobe) and two O atoms of a bicarbonate ion bind to an Al^{3+} ion with distorted octahedral-like symmetry in the closed inter-domain cleft of either lobe. These ligands for Al^{3+} are exactly the same as those for Fe^{3+} and the associated bicarbonate anions are also bound identically. In Fig. 2, which shows the domain-opened structure of the apo form and the closed structures of the metal-bound (Al^{3+} and Fe^{3+}) forms, Al^{3+}-bound oTf seems to have slightly narrower metal-binding clefts than the Fe^{3+}-bound form. The widths of the metal-binding clefts were quantitatively evaluated by the distances between the centres of gravity of the two domains forming the clefts, since the lines connecting the centres of domain 1 and domain 2 pass through the clefts in both lobes. The distances between the centres of the two domains (the widths of the clefts) of the Al^{3+}-bound form (N-lobe, 23.6 Å; C-lobe, 22.9 Å) and the Fe^{3+}-bound form (N-lobe, 24.0 Å; C-lobe, 23.4 Å) are much smaller than those of apo form (N-lobe, 30.4 Å; C-lobe, 27.8 Å). The distances between the domains appear to be slightly smaller in the Al^{3+}-bound form than in the Fe^{3+}-bound form; however, the differences are considered to be within the range of experimental error considering the resolution of the Fe^{3+}-bound structure (2.4 Å). For further analysis, a high-resolution structure of the Fe^{3+}-bound form is necessary. In the current structure, the smaller size of the Al^{3+} ion (radius 0.54 Å) compared with the Fe^{3+} ion (0.65 Å) is the main cause of the shorter bonds between Al^{3+} and the O atoms of the Asp ligands (1.94 Å in the N-lobe; 1.95 Å in the C-lobe) compared with the equivalent bonds to Fe^{3+} in the Fe^{3+}-bound form (2.18 Å in the N-lobe; 2.34 Å in the C-lobe). Fig. 2 also demonstrates that the relative orientations of the N- and C-lobes are almost the same in both the Al^{3+}- and Fe^{3+}-bound forms.

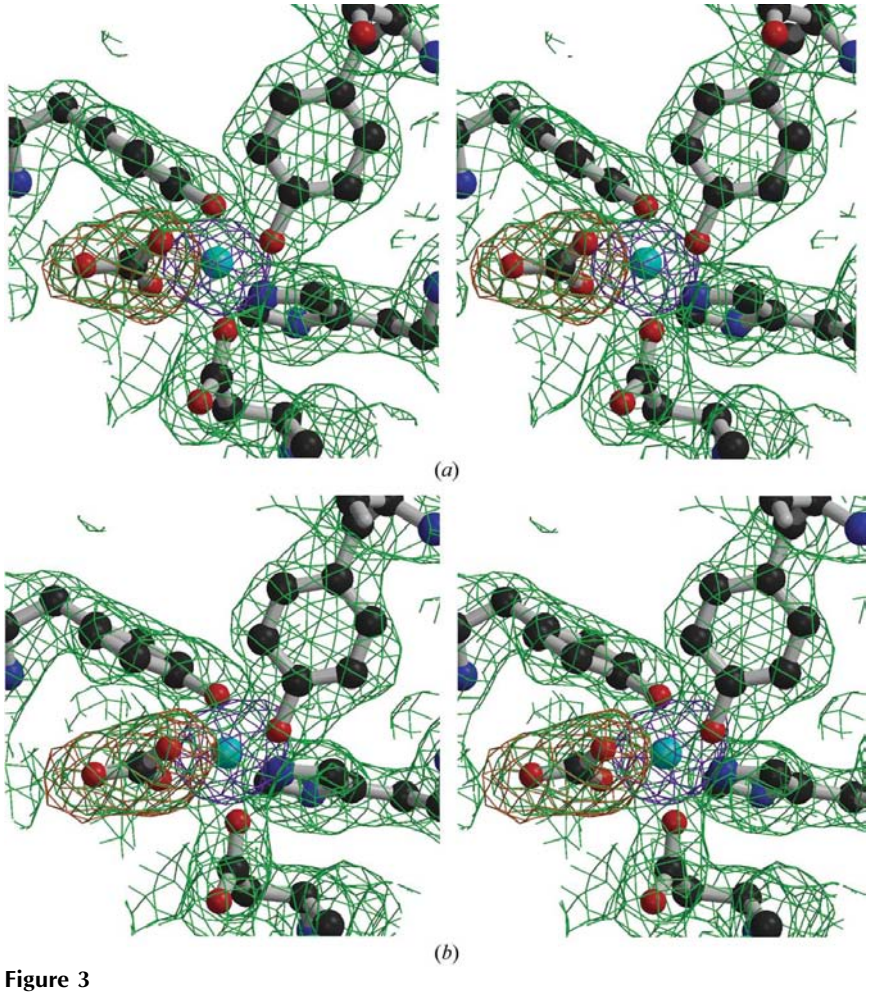

Figure 3
Stereo diagrams depicting the aluminium-binding sites. Electron-density maps ($2F_o - F_c$, contoured at 1σ; green) are shown for the Al^{3+}-binding sites in (*a*) the N-lobe and (*b*) the C-lobe. Electron-density omit maps ($F_o - F_c$, contoured at 3σ; purple and orange) were calculated after refinement using a model in which Al^{3+} ions or bicarbonate anions were omitted. The final model is superimposed in a stick presentation with atoms in standard colours for the Al^{3+}-coordinating residues (Asp60, Tyr92, Tyr191 and His250 for the N-lobe; Asp395, Tyr431, Tyr524 and His592 for the C-lobe) and bicarbonate anions. Al^{3+} atoms are shown by small spheres coloured cyan. The figures were prepared with the programs *BobScript* (Esnouf, 1999) and *Raster3D* (Merritt & Bacon, 1997).

Transferrin binds Al^{3+} with lower binding constants ($\log K_1 = 13.5$ and $\log K_2 = 12.5$ for binding to the C- and N-lobes of human transferrin, respectively) than those for Fe^{3+} ($\log K_1 = 22.5$ and $\log K_2 = 21.4$) (Aisen *et al.*, 1978; Martin *et al.*, 1987; Harris & Sheldon, 1990). Our calorimetric result (Fig. 1) confirms that transferrin can bind Al^{3+} instead of Fe^{3+}, with a smaller ΔT_m (difference in the thermal transition temperature between the metal-binding form and the apo form) of the Al^{3+}-bound form (6.6 K) compared with the Fe^{3+}-bound form (22.0 K), which is mainly related to the different binding constants of these metal ions (Brandts & Lin, 1990). Harris & Sheldon (1990) and Martin (1988) have discussed the binding of Al^{3+} to transferrin in terms of the binding constants of Al^{3+} and Fe^{3+} to various low-molecular-weight chelating agents. Generally, the binding constants for Al^{3+} are smaller than those for Fe^{3+} and a plot of the logarithms of the binding constants of Al^{3+} (y axis) and Fe^{3+} (x axis) can be fitted to a linear regression with a slope less than 1.0 (a linear free-energy relationship; LFER; Harris & Sheldon, 1990). The binding constants of Al^{3+} and Fe^{3+} to transferrin agree with this plot when the pK_a values of the two Tyr ligands are considered (Martin, 1988), which indicates that the metal-binding residues of transferrin effectively surround the Al^{3+} ions as small chelating agents. In the current structure, as already shown, the bond distances between the Al^{3+} and Asp residues are smaller than distances between Fe^{3+} and

Asp, enabling the effective binding of Al^{3+} despite their smaller ionic radius. As shown in this crystal structure, the substitution of Fe^{3+} by Al^{3+} does not disrupt the inter-domain contacts which stabilize the domain-closed form. This is also one of the reasons why the binding of Al^{3+} and transferrin is not weak compared with other chelating agents: binding constants of Al^{3+} are in the range of LFER. For oTf, Fe^{3+} preferentially binds to the N-lobe (Yamamura *et al.*, 1985; Ichimura *et al.*, 1989; Okamoto *et al.*, 2004), in contrast to the C-lobe preference of human transferrin. As shown here, the coordination is slightly more distorted from octahedral symmetry in the C-lobe than the N-lobe and the *B* factor of the Al atom in the C-lobe (21.2 $Å^2$) is much larger than that in the N-lobe (12.0 $Å^2$). These are consistent with the N-lobe preference for Al^{3+} binding of oTf.

The recent structure of the transferrin receptor–transferrin complex has revealed that transferrin interacts with transferrin receptor through its domains N1, N2 and C1 (Cheng *et al.*, 2004); the transferrin receptor recognizes the domain-closed structure of the N-lobe by interactions involving both domains of the N-lobe. In spite of small differences, the Al^{3+}-bound form and Fe^{3+}-bound form have similar domain-closed structures. This highly similar structure for Al^{3+}-bound transferrin may permit it to bind to the transferrin receptor. The dilysine trigger (Lys209 NZ$\cdots$Lys301 NZ) in the N-lobe, an unusual interaction which facilitates iron release at low pH (Dewan *et al.*, 1993), is also found in the Al^{3+}-bound form with an identical bond distance (2.86 Å). This dilysine trigger may therefore also facilitate the release of Al^{3+} at low pH in the endosome. These findings support the participation of transferrin in the transportation of Al^{3+} ions *in vivo* as proposed by Roskams & Connor (1990).

This work was supported by a Grant-in-Aid for Young Scientists from the Ministry of Education, Culture, Sports, Science and Technology. The synchrotron-radiation experiments were performed at BL38B1 of SPring-8 with the approval of the Japan Synchrotron Radiation Research Institute (JASRI; proposal No. 2005A0927-RL1-np). We thank Dr Atsuo Suzuki (Graduate School of Engineering, Nagoya University, Japan) for his advice on data collection and processing.

References

Aisen, P., Leibman, A. & Zweier, J. (1978). *J. Biol. Chem.* **253**, 1930–1937.
Aisen, P. & Listowsky, I. (1980). *Annu. Rev. Biochem.* **49**, 357–393.
Anderson, B. F., Baker, H. M., Norris, G. E., Rumball, S. V. & Baker, E. N. (1990). *Nature (London)*, **344**, 784–787.
Baker, H. M., Anderson, B. F. & Baker, E. N. (2003). *Proc. Natl Acad. Sci. USA*, **100**, 3579–3583.
Baker, H. M., Baker, C. J., Smith, C. A. & Baker, E. N. (2000). *J. Biol. Inorg. Chem.* **5**, 692–698.
Brandts, J. F. & Lin, L. N. (1990). *Biochemistry*, **29**, 6927–6940.
Brown-Mason, A. & Woodworth, R. C. (1984). *J. Biol. Chem.* **259**, 1866–1873.
Brünger, A. T., Adams, P. D., Clore, G. M., DeLano, W. L., Gros, P., Grosse-Kunstleve, R. W., Jiang, J.-S., Kuszewski, J., Nilges, M., Pannu, N. S., Read, R. J., Rice, L. M., Simonson, T. & Warren, G. L. (1998). *Acta Cryst.* D**54**, 905–921.
Cheng, Y., Zak, O., Aisen, P., Harrison, S. C. & Walz, T. (2004). *Cell*, **116**, 565–576.
Collaborative Computational Project, Number 4 (1994). *Acta Cryst.* D**50**, 760–763.
Congiu-Castellano, A., Boffi, F., Della Longa, S., Giovannelli, A., Girasole, M., Natali, F., Pompa, M., Soldatov, A. & Bianconi, A. (1997). *Biometals*, **10**, 363–367.
Corain, B., Bombi, G. G., Tapparo, A., Perazzolo, M. & Zatta, P. (1996). *Coord. Chem. Rev.* **149**, 11–22.
Dautry-Varsat, A., Ciechanover, A. & Lodish, H. F. (1983). *Proc. Natl Acad. Sci. USA*, **80**, 2258–2262.
Dean, J. A. (1999). *Lange's Handbook of Chemistry*, 15th ed. New York: McGraw–Hill.
Dewan, J. C., Mikami, B., Hirose, M. & Sacchettini, J. C. (1993). *Biochemistry*, **32**, 11963–11968.
Emsley, P. & Cowtan, K. (2004). *Acta Cryst.* D**60**, 2126–2132.
Esnouf, R. M. (1999). *Acta Cryst.* D**55**, 938–940.
Gerstein, M., Anderson, B. F., Norris, G. E., Baker, E. N., Lesk, A. M. & Chothia, C. (1993). *J. Mol. Biol.* **234**, 357–372.
Guha Thakurta, P., Choudhury, D., Dasgupta, R. & Dattagupta, J. K. (2003). *Acta Cryst.* D**59**, 1773–1781.
Harris, W. R. & Sheldon, J. (1990). *Inorg. Chem.* **29**, 119–124.
Ichimura, K., Kihara, H., Yamamoto, K. & Satake, K. (1989). *J. Biochem. (Tokyo)*, **106**, 50–54.
Klausner, R. D., Ashwell, G., van Renswoude, J., Harford, J. B. & Bridges, K. R. (1983). *Proc. Natl Acad. Sci. USA*, **80**, 2263–2266.
Kraulis, P. J. (1991). *J. Appl. Cryst.* **24**, 946–950.
Kurokawa, H., Dewan, J. C., Mikami, B., Sacchettini, J. C. & Hirose, M. (1999). *J. Biol. Chem.* **274**, 28445–28452.
Kurokawa, H., Mikami, B. & Hirose, M. (1995). *J. Mol. Biol.* **254**, 196–207.
Li, H., Sadler, P. J. & Sun, H. (1996). *J. Biol. Chem.* **271**, 9483–9489.
Martin, R. B. (1988). *Metal Ions in Biological Systems*, Vol. 24, edited by H. Sigel, pp. 1–57. New York: Marcel Dekker.
Martin, R. B., Savory, J., Brown, S., Bertholf, R. L. & Wills, M. R. (1987). *Clin. Chem.* **33**, 405–407.
Mason, A. B., Brown, S. A. & Church, W. R. (1987). *J. Biol. Chem.* **262**, 9011–9015.
Mason, A. B., Woodworth, R. C., Oliver, R. W., Green, B. N., Lin, L. N., Brandts, J. F., Savage, K. J., Tam, B. M. & MacGillivray, R. T. (1996). *Biochem. J.* **319**, 361–368.
Merritt, E. A. & Bacon, D. J. (1997). *Methods Enzymol.* **277**, 505–524.
Mizutani, K., Mikami, B. & Hirose, M. (2001). *J. Mol. Biol.* **309**, 937–947.
Mizutani, K., Yamashita, H., Kurokawa, H., Mikami, B. & Hirose, M. (1999). *J. Biol. Chem.* **274**, 10190–10194.
Mizutani, K., Yamashita, H., Mikami, B. & Hirose, M. (2000). *Biochemistry*, **39**, 3258–3265.
Oe, H., Doi, E. & Hirose, M. (1988). *J. Biochem. (Tokyo)*, **103**, 1066–1072.
Okamoto, I., Mizutani, K. & Hirose, M. (2004). *Biochemistry*, **43**, 11118–11125.
Roskams, A. J. & Connor, J. R. (1990). *Proc. Natl Acad. Sci. USA*, **87**, 9024–9027.
Sharma, A. K. & Singh, T. P. (1999). *Acta Cryst.* D**55**, 1799–1804.
Smith, C. A., Anderson, B. F., Baker, H. M. & Baker, E. N. (1992). *Biochemistry*, **31**, 4527–4533.
Thakurta, P. G., Choudhury, D., Dasgupta, R. & Dattagupta, J. K. (2004). *Biochem. Biophys. Res. Commun.* **316**, 1124–1131.
Thibodeau, S. N., Lee, D. C. & Palmiter, R. D. (1978). *J. Biol. Chem.* **253**, 3771–3774.
Yamamura, T., Shimo, S., Tsuda, T. & Satake, K. (1985). *Rep. Prog. Polym. Phys. Jpn*, **28**, 633–636.
Young, S. P., Bomford, A. & Williams, R. (1984). *Biochem. J.* **219**, 505–510.